THE JOURNAL OF BIOLOGICAL CHEMISTRY VOL. 286, NO. 31, pp. 27612–27621, August 5, 2011

Retuning Rieske-type Oxygenases to Expand Substrate Range*

Received for publication, April 27, 2011, and in revised form, May 25, 2011 Published, JBC Papers in Press, June 8, 2011, DOI 10.1074/jbc.M111.255174

Mahmood Mohammadi[‡1], Jean-François Viger[‡1], Pravindra Kumar[§¶1], Diane Barriault[‡], Jeffrey T. Bolin[§], and Michel Sylvestre[‡2]

From the [‡]Institut National de la Recherche Scientifique-Institut Armand-Frappier, Laval, Quebec H7V 1B7, Canada, the [§]Department of Biological Sciences and Center for Cancer Research, Purdue University, West Lafayette, Indiana 47907, and the [¶]Department of Biotechnology, Indian Institute of Technology, Roorkee 247667, India

Rieske-type oxygenases are promising biocatalysts for the destruction of persistent pollutants or for the synthesis of fine chemicals. In this work, we explored pathways through which Rieske-type oxygenases evolve to expand their substrate range. $BphAE_{p4}$, a variant biphenyl dioxygenase generated from *Burkholderia xenovorans* LB400 $BphAE_{LB400}$ by the double substitution T335A/F336M, and $BphAE_{RR41}$, obtained by changing Asn^{338}, Ile^{341}, and Leu^{409} of $BphAE_{p4}$ to Gln^{338}, Val^{341}, and Phe^{409}, metabolize dibenzofuran two and three times faster than $BphAE_{LB400}$, respectively. Steady-state kinetic measurements of single- and multiple-substitution mutants of $BphAE_{LB400}$ showed that the single T335A and the double N338Q/L409F substitutions contribute significantly to enhanced catalytic activity toward dibenzofuran. Analysis of crystal structures showed that the T335A substitution relieves constraints on a segment lining the catalytic cavity, allowing a significant displacement in response to dibenzofuran binding. The combined N338Q/L409F substitutions alter substrate-induced conformational changes of protein groups involved in subunit assembly and in the chemical steps of the reaction. This suggests a responsive induced fit mechanism that retunes the alignment of protein atoms involved in the chemical steps of the reaction. These enzymes can thus expand their substrate range through mutations that alter the constraints or plasticity of the catalytic cavity to accommodate new substrates or that alter the induced fit mechanism required to achieve proper alignment of reaction-critical atoms or groups.

Rieske-type oxygenases (ROs)[3] catalyze a stereospecific oxygenation of many aromatic and hetero-aromatic molecules. These enzymes have potential applications as biocatalysts to degrade persistent pollutants, such as polyaromatic hydrocarbons (1, 2), polychlorinated biphenyls (3–5), and chlorodibenzofurans (6, 7), or to produce chiral arene *cis*-dihydrodiols of interest in enantioselective syntheses for the manufacture of fine chemicals (8–10). Biphenyl dioxygenase, one of the most extensively studied ROs, catalyzes the first reaction of the bacterial biphenyl catabolic pathway. Biphenyl dioxygenase has three components: the iron-sulfur oxygenase (hereinafter referred to as BphAE), a heterohexamer comprised of three α (M_r = 51,000) and three β (M_r = 22,000) subunits; the ferredoxin (BphF, M_r = 12,000); and the ferredoxin reductase (BphG, M_r = 43,000). The encoding genes for *Burkholderia xenovorans* LB400 (11), which is the best polychlorinated biphenyl degrader of natural origin, are *bphA* ($BphAE_{LB400}$ α subunit), *bphE* ($BphAE_{LB400}$ β subunit), *bphF* ($BphF_{LB400}$), and *bphG* ($BphG_{LB400}$) (see Fig. 1).

$BphAE_{LB400}$ has been thoroughly investigated because it can oxygenate a broad range of substrates. $BphAE_{LB400}$ variants with extended substrate range have been generated by site-directed mutagenesis (12) and directed evolution (13, 14). However, the enzyme's structural features that modulate substrate range and catalytic efficiency have yet to be determined. Many investigations have identified residues in contact with the substrate, or removed from it, as key determinants of substrate preference and regiospecificity (12–23). Recently Thr^{335} of $BphAE_{LB400}$, which is removed from the substrate, was found to restrain the range of chlorobiphenyls the enzyme can oxidize by controlling the spatial distribution of protein atoms in contact with the substrates (17). Changing Thr^{335} to Ala relieves intramolecular constraints on Gly^{321}, allowing for significant movement of this residue during substrate binding, thereby increasing the space available to accommodate the bulkier substrate 2,6-dichlorobiphenyl. In addition, crystal structures of the oxygenase component of carbazole 1,9a-dioxygenase and of the binary complex of the oxygenase and ferredoxin components provided evidence that conformational changes are required to suitably align the Rieske clusters of the ferredoxin and oxygenase components (24). These observations are consistent with a mechanism whereby an induced fit process is involved in RO substrate binding and catalytic function. Understanding how conformational adjustments influence the turnover rate and how they can be modified to enhance activity toward new substrates will aid the development of new, better performing catalysts.

Unlike biphenyl, the fused rings of dibenzofuran are locked in a co-planar conformation (Fig. 1), and this molecule is poorly oxygenated by $BphAE_{LB400}$ (25, 26). In previous reports (7, 14),

* This work was supported by Natural Sciences and Engineering Research Council of Canada Grant RGPIN/39579-2007 and an Indian Department of Science and Technology young scientist grant (to P. K.).

The atomic coordinates and structure factors (codes 2YFI and 2YFJ) have been deposited in the Protein Data Bank, Research Collaboratory for Structural Bioinformatics, Rutgers University, New Brunswick, NJ (http://www.rcsb.org/).

[1] These authors contributed equally to this work.

[2] To whom correspondence should be addressed: INRS-Institut Armand-Frappier, Laval, Québec H7V 1B7, Canada. Tel.: 450-687-5010; Fax: 450-686-5501; E-mail: Michel.Sylvestre@iaf.inrs.ca.

[3] The abbreviations used are: RO, Rieske-type oxygenase; IPTG, isopropyl β-D-thiogalactopyranoside; MES, 4-morpholineethanesulfonic acid.

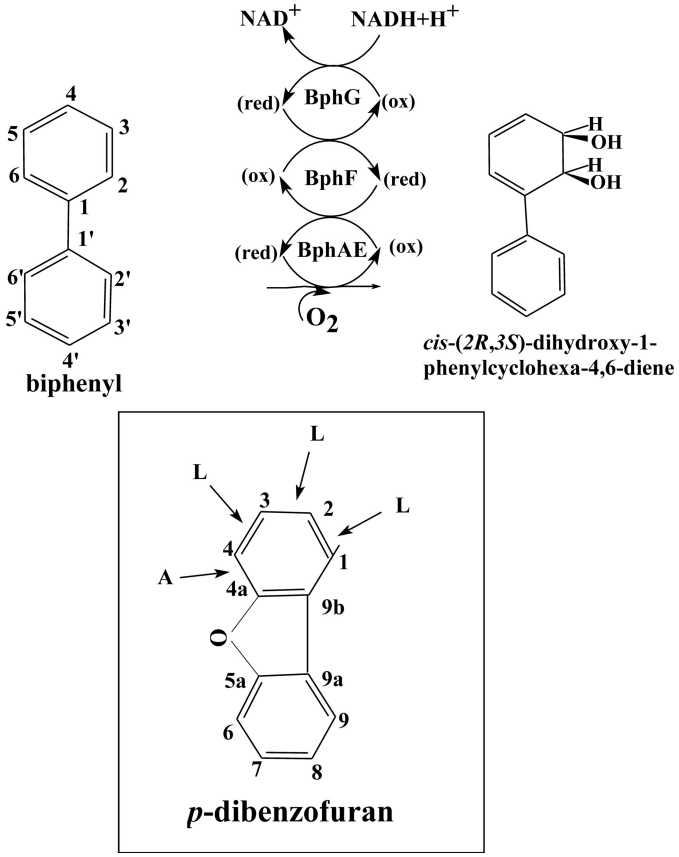

FIGURE 1. **Biphenyl dioxygenase reaction.** The *inset* shows the structure of dibenzofuran and possible positions of oxygenation. *A*, angular; *L*, lateral.

we described variant $BphAE_{p4}$ obtained by the double substitution of Thr^{335}-Phe^{336} of $BphAE_{LB400}$ to Ala^{335}-Met^{336} and variant $BphAE_{RR41}$ obtained by changing Asn^{338}, Ile^{341}, and Leu^{409} of $BphA_{p4}$ to Gln^{338}, Val^{341}, and Phe^{409}. $BphAE_{RR41}$ was selected by directed evolution for its higher turnover rate with dibenzofuran than the parent $BphAE_{p4}$ (7). The library was produced by changing Asn^{338} and Ile^{341} of $BphAE_{p4}$ simultaneously by saturation mutagenesis (7), but an additional spontaneous mutation L409F occurred in this mutant.

In this study, to gain more insight into the pathways through which ROs evolve to expand their substrate range, we identified the mutations in $BphAE_{p4}$ and in $BphAE_{RR41}$ that contribute most to their enhanced activity toward dibenzofuran and analyzed the crystal structures of $BphAE_{RR41}$ and its dibenzofuran-bound form to evaluate the consequences of the mutations.

EXPERIMENTAL PROCEDURES

Strains and Plasmids—Escherichia coli DH11S (27) and C41(DE3) (28) (Statagene, La Jolla, CA) were used in this study. The WT $BphAE_{LB400}$ and its mutants $BphAE_{p401}$ (T335A), $BphAE_{p402}$ (F336M), $BphAE_{p4}$ (T335A/F336M), and $BphAE_{RR41}$ (T335A/F336M/N338Q/I341V/L409F) were described previously (17).

A previously described two-step site-directed mutagenesis protocol (7) was used to create a set of mutants representing the six mutants that can be produced by single and double substitutions of N338Q, I341V, and L309F of $BphAE_{p4}$ (Table 1). These *bphAE* mutants were cloned in pQE31 or in pET14b.

TABLE 1
Sequence pattern of $BphAE_{LB400}$ variants

Protein designation	Residue position[a]				
	335	336	338	341	409
$BphAE_{LB400}$	T	F	N	I	L
	A	F	N	I	L
	T	M	N	I	L
$BphAE_{p4}$	A	M	N	I	L
	A	M	Q	I	L
	A	M	N	V	L
	A	M	N	I	F
	A	M	Q	V	L
	A	M	N	V	F
	A	M	Q	I	F
$BphAE_{RR41}$	A	M	Q	V	F

[a] All other residues for these variants are identical to those of $BphAE_{LB400}$.

DNA protocols were generally according to Sambrook *et al.* (29). DNA from each mutant was sequenced at the Genome Quebec DNA Sequencing Center (Montreal, Canada). Biphenyl and dibenzofuran were of the highest purity grade available from AccuStandard (New Haven, CT).

Protein Analysis—The level of expression of each variant enzyme in IPTG-induced *E. coli* DH11S pDB31[LB400-*bphFG*] + pQE31[*bphAE*] was assessed by SDS-PAGE (30) of crude cell extracts prepared under benign (cells were sonicated in 10 mM phosphate buffer, pH 7.3, containing 140 mM NaCl) or denaturating conditions (cells were sonicated in 10 mM phosphate buffer, pH 7.3, containing 140 mM NaCl and 8 M urea). The gels were stained with Coomassie Brilliant Blue. Purified enzyme preparations were also analyzed by HPLC gel filtration chromatography using a Waters Protein Pak 300 SW column (7.8 × 300 mm), as described previously (31).

Monitoring Enzyme Activity with Purified Enzyme Preparations—Reconstituted His-tagged purified biphenyl dioxygenase preparations were used to monitor enzyme activity and metabolite production. In this case, the genes expressing each enzyme component were cloned into pET-14b (Novagen, Madison, WI) and expressed in *E. coli* C41(DE3). The components were produced as recombinant His-tagged protein and purified by affinity chromatography on high performance nickel-Sepharose resin (GE Healthcare) (7). The concentration of each purified component was determined by spectrophotometry (31–33). Enzymatic reactions were performed as described previously (7) at 37 °C, in 50 mM pH 6.0 MES buffer, and in a volume of 400 μl containing 1.2 nmol of each of the His-tagged enzyme component and 200 nmol of NADH. Substrate depletion and metabolite production were analyzed and quantified by GC-MS using previously published protocols (7). The steady-state kinetic parameters of all BphAEs were determined by recording oxygen consumption rates using a Clarke-type Hansatech model DW1 oxygraph (34) for concentrations of biphenyl and dibenzofuran varying between 5 and 150 μM. Kinetic parameters reported in this investigation were obtained from analysis of at least two independently produced preparations tested in triplicate.

Crystal Structure Analyses—Purification, crystallization, and preliminary x-ray diffraction properties of $BphAE_{RR41}$ have been communicated elsewhere (35). The procedures to prepare crystals of $BphAE_{RR41}$ and its dibenzofuran-bound form were identical to those described for $BphAE_{p4}$ (17). The crystal struc-

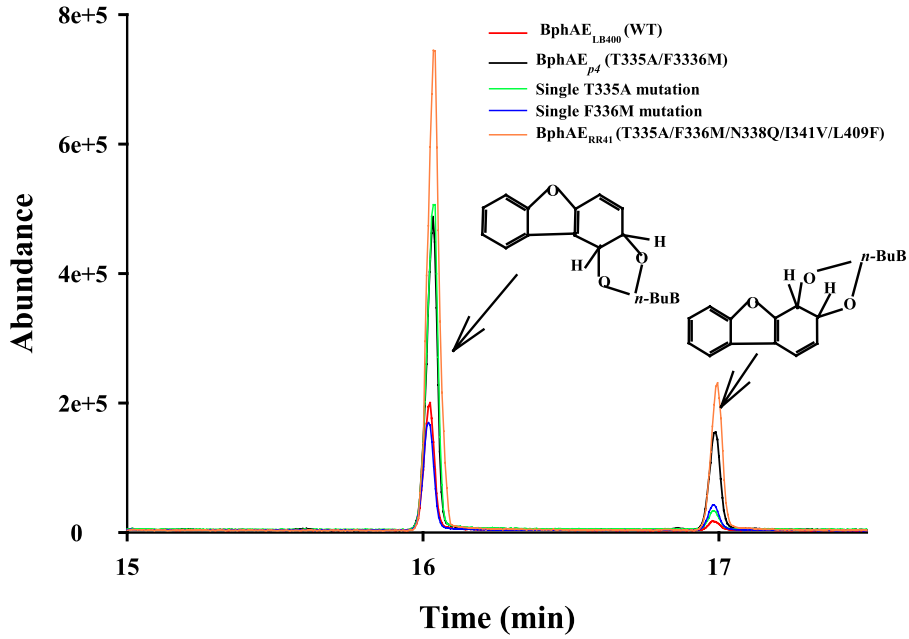

FIGURE 2. **GC-MS spectra showing the relative amounts of the dihydrodihydroxy metabolites produced from dibenzofuran by BphAE$_{LB400}$ and its variants.** 1.2 nmol of each purified enzyme preparation was incubated for 2 min under the conditions described under "Experimental Procedures." The metabolites were extracted and derivatized with butylboronate before analysis by GC-MS.

TABLE 2

Steady-state kinetic parameters of BPDO variants

The steady-states kinetics were determined from the oxygen consumption rates as described under "Experimental Procedures."

Substrate	BphAE$_{LB400}$ WT	T335A	F336M	BpbAE$_{p4}$ T335A/F336M	I341V[a]	I341V/L409F[a]	N338Q/L409F[a]	BphAE$_{RR41}$ N338Q/I341V/L409F[a]
Biphenyl								
K_m (μM)	22 (0.0)	30 (4.0)	17 (5.0)	33 (1.4)	32.5 (2.0)	21.5 (0.7)	32.0 (0.0)	34.5 (6.3)
k_{cat} (s^{-1})	0.9 (0.1)	1.1 (0.0)	0.4 (0.1)	1.0 (0.1)	0.7 (0.1)	0.8 (0.1)	1.5 (0.1)	1.3 (0.3)
k_{cat}/K_m (10^3 M^{-1} s^{-1})	41 (6.0)	36 (5.0)	23 (0.1)	31 (4)	21 (0.5)	37 (3.0)	46 (4.0)	38 (0.0)
Dibenzofuran								
K_m (μM)	19.5 (0.7)	19 (0.6)	19 (1)	20 (1.4)	25 (9.9)	21.5 (2.1)	23 (7.8)	22.0 (0.0)
k_{cat} (s^{-1})	0.12 (0.0)	0.22 (0.0)	0.12 (0.05)	0.26 (0.01)	0.17 (0.07)	0.22 (0.02)	0.5 (0.05)	0.38 (0.08)
k_{cat}/K_m (10^3 M^{-1} s^{-1})	6 (0.0)	12 (2.0)	6 (0.07)	13 (2.0)	7 (0.1)	10 (0.1)	22 (5)	17 (4.0)

[a] These mutants carry also the double T335A/F336M mutation.

tures were obtained and analyzed using the same approaches and software used in studies of BphAE$_{p4}$ (17). Crystal structures of BphAE$_{RR41}$ and its dibenzofuran-bound form were compared with crystal structures of BphAE$_{LB400}$ (RCSB Protein Data Bank accession code 2XR8) and its biphenyl-bound form (code 2XRX), as well as BphAE$_{p4}$ (code 2XSO) and its 2,6-dichlorobiphenyl-bound form (code 2XSH).

Protein Data Bank Accession Codes—The coordinates have been deposited with the RCSB Protein Data Bank under accession codes 2YFI for BphAE$_{RR41}$ and 2YFJ for its complex with dibenzofuran.

RESULTS

Steady-state Kinetics of BphAE$_{p4}$, BphAE$_{RR41}$, and Their Variants with Dibenzofuran—Based on the sum of areas under GC-MS peaks of metabolites produced when 1.2 nmol of enzyme was incubated for 2 min with 100 μM dibenzofuran, BphAE$_{p4}$ and BphAE$_{RR41}$ produced, respectively, three and four times more metabolites than BphAE$_{LB400}$ (Fig. 2). Consistent with the single time point measurements, the apparent k_{cat} value for BphAE$_{RR41}$ is ~1.5 times higher than that of BphAE$_{p4}$ and 3 times higher than for BphAE$_{LB400}$ based on the oxygen consumption rates recorded for variable concentrations of dibenzofuran (Table 2). These results show the superior ability to metabolize dibenzofuran of BphAE$_{RR41}$ compared with BphAE$_{p4}$ and BphAE$_{LB400}$.

To identify the mutations that contribute most to the enhanced activity of BphAE$_{p4}$ and BphAE$_{RR41}$ toward dibenzofuran, we assayed all mutants carrying single or multiple mutations at positions 335, 336, 338, 341, and 409 (Table 1). Based on the sum of areas under GC-MS peaks, the amounts of metabolites produced by the T335A mutant and by BphAE$_{p4}$ (T335A/F336M) were similar and about three times higher than the amounts for BphAE$_{LB400}$ and its F336M mutant (Fig. 2). The superior ability of the T335A mutant to metabolize dibenzofuran was confirmed by steady-state kinetics (Table 2). Furthermore, the single F336M substitution lowered k_{cat} and k_{cat}/K_m for the reaction with biphenyl. This identified the T335A substitution as responsible for the enhanced ability of BphAE$_{p4}$ to metabolize dibenzofuran.

The apparent k_{cat} values for the mutants T335A/F336M/I341V and T335A/F336M/I341V/L409F toward biphenyl and dibenzofuran were lower than for BphAE$_{p4}$. In addition, introducing the single I341V or the double I341V/L409F mutations

into $BphAE_{p4}$ did not contribute to enhanced activity toward dibenzofuran. We did not determine steady-state kinetic parameters for variant T335A/F336M/L409F. However, the observation that recombinant *E. coli* cells producing this enzyme did not degrade dibenzofuran more efficiently than $BphAE_{p4}$ (not shown) indicates that changing Leu^{409} of $BphAE_{p4}$ to Phe did not influence activity toward dibenzofuran. Variants T335A/F336M/N338Q and T335A/F336M/N338Q/I341V were poorly active toward biphenyl and dibenzofuran because they are not assembled correctly (see below). The steady-state kinetic parameters obtained with these two variants were too difficult to determine accurately and therefore are not reported here. On the other hand, the apparent k_{cat} value for T335A/F336M/N338Q/L409F toward dibenzofuran was in the same range or even higher than for $BphAE_{RR41}$ (T335A/F336M/N338Q/I341V/L409F) (Table 2). Furthermore, replacing Asn^{338} and Leu^{409} of $BphAE_{p4}$ with Gln^{338} and Phe^{409} created a double mutant exhibiting enhanced activity toward dibenzofuran.

The Poor Activity of Variants T335A/F336M/N338Q and T335A/F336M/N338Q/I341V Is the Result of Hexamer Misassembly—Unlike $BphAE_{RR41}$ and T335A/F336M/N338Q/L409F, variants T335A/F336M/N338Q and T335A/F336M/N338Q/I341V were poorly active, which suggests a detrimental effect of the N338Q substitution on enzyme activity. When the proteins of IPTG-induced recombinant *E. coli* cells producing variant BphAEs were extracted under denaturing conditions and separated by SDS-PAGE, the intensities of bands corresponding to the α and β subunits were similar for all strains (Fig. 3*A*). This shows that the level of expression of BphAE is similar for all IPTG-induced *E. coli* clones expressing these variants. However, analysis of cell extracts prepared under nondenaturing conditions revealed significantly lower intensities of the bands corresponding to the α subunits for variant T335A/F336M/N338Q and T335A/F336M/N338Q/I341V compared with the other variants (Fig. 3*B*). This suggests misassembly or early dissociation of $\alpha_3\beta_3$ hexamers resulting in a loss of α subunits into the nonsoluble protein fraction. HPLC gel filtration analysis of freshly purified His-tagged BphAE of variants T335A/F336M/N338Q and T335A/F336M/N338Q/I341V confirmed that less than 10% of each protein preparation exhibited the expected $\alpha_3\beta_3$ association pattern (not shown). Therefore, the N338Q substitution hinders hexamer assembly unless a concomitant L409F substitution is introduced. Nevertheless, the double N338Q/L409F substitution is beneficial for enhancing catalytic properties toward dibenzofuran.

Overall Structure of $BphAE_{RR41}$—The overall structures of $BphAE_{RR41}$ and its dibenzofuran-bound form are very similar to the crystal structures of the $BphAE_{p4}$:2,6-dichlorobiphenyl complex (17), which contains triplets of $\alpha\beta$ dimers associated into two hexamers in the asymmetric unit (chains ABCDEF and chains GHIJKL). For both structures, the final refined models contain residues Asn^{18} to Phe^{143} plus Phe^{153} to Pro^{459} of each α subunit, residues Phe^{9} to Phe^{188} of each β subunit and 1217 water molecules. The diffraction data and refined models are characterized in Table 3.

Superposition of all C^{α} atoms for the $\alpha\beta$ dimer of chains AB with chains CD-KL yielded rmsd values of 0.2–0.3 Å. The

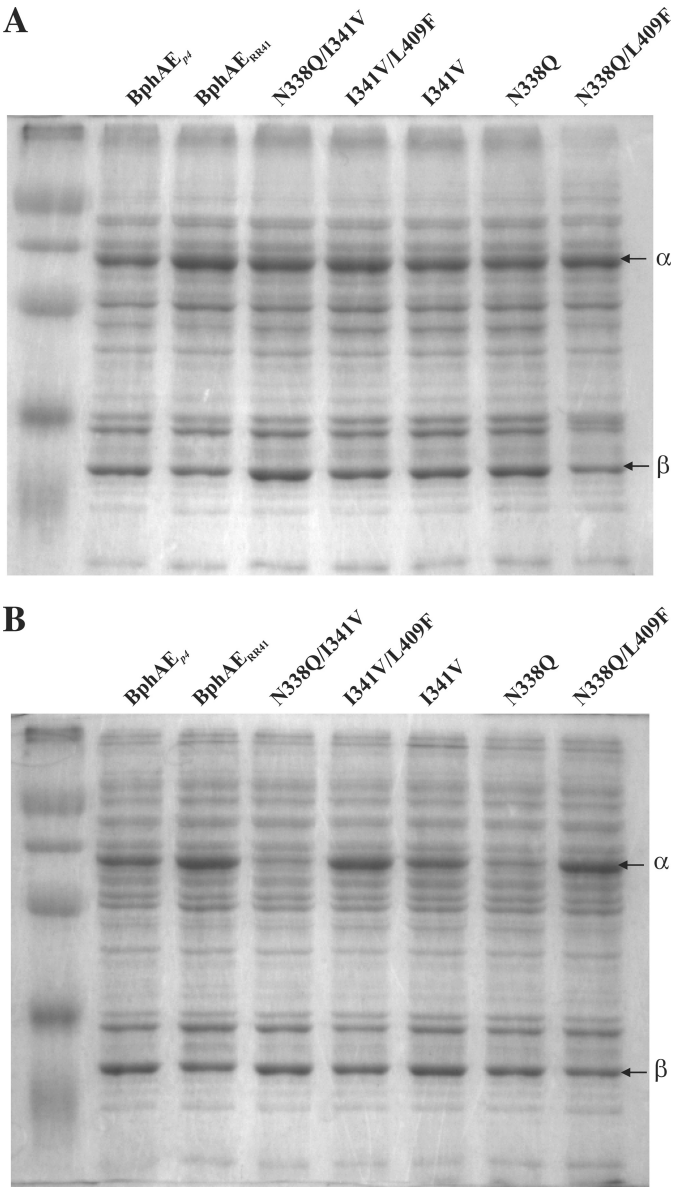

FIGURE 3. **SDS-PAGE of lyzates of IPTG-induced *E. coli* cells expressing the indicated variants derived from $BphAE_{p4}$ (T335A/F336M).** *A*, gel of the indicated protein extracts prepared under denaturing conditions. *B*, gel of the indicated protein extracts prepared under nondenaturing conditions. In addition to the indicated substitutions, all of the mutants in the *fourth lane* through the *eighth lane* carry the double T336A/F336M mutation. The *far-left lane* is the molecular weight marker. The bands corresponding to the α and β subunits are marked by *arrows*.

poorly ordered residues and protein segments were the same as observed for $BphAE_{p4}$ (17), including segments comprising residues Ile^{247} to Lys^{263} and Glu^{280} to Val^{287} of the α subunit and residues 9–17 and 158–164 of the β subunit. In the $BphAE_{RR41}$-dibenzofuran complex structure, dibenzofuran could be identified clearly in $F_o - F_c$ difference Fourier maps in all active sites of the ABCDEF hexamer. Similar to $BphAE_{LB400}$-biphenyl, a water molecule lies between the Fe^{2+} and dibenzofuran at ~2 Å from the catalytic iron. Electron density maps of the active site residues of the $BphAE_{RR41}$ and of its dibenzofuran-bound form are shown for dimer AB in Fig. 4.

When the $BphAE_{RR41}$-dibenzofuran $BphAE_{LB400}$-biphenyl structures are superposed, the positions of the carbons targeted

for hydroxylation, C-4a and C-4 of dibenzofuran and C-2 and C-3 of biphenyl, are nearly the same in $\alpha\beta$ dimers AB, CD, and EF (not shown). In $\alpha\beta$ dimers AB, CD, and EF of $BphAE_{RR41}$-dibenzofuran, the substrate is in an orientation that would favor 4,4a angular attack. This is unexpected because biochemical data revealed dioxygenation of the lateral 1,2 and 3,4 carbons of dibenzofuran as by far most favored for $BphAE_{RR41}$ (7). In the crystal structure, the furan ring's oxygen atom contacts the water ligand of the active site Fe^{2+} atom. Based on observations drawn from the naphthalene dioxygenase crystal structure, Karlsson *et al.* (36) proposed a reaction cycle for ROs in which Fe^{2+} coordinates this water in states prior to dioxygen binding. When dioxygen binds, it intercalates side-on between the iron and the substrate displacing the water. Thus, a subsequent adjustment in substrate position or orientation is possible such that the lateral attack would occur. In essence, the dibenzofuran-O-water interaction seen in the crystal form could produce a false inference about the points of attack because the structure reports on a state prior to dioxygen binding.

TABLE 3
Crystallographic data and refinement results for $BphAE_{RR41}$ structure

	$BphAE_{RR41}$	$BphAE_{RR41}$:dibenzofuran
Crystallographic data		
Space group	$P2_1$	$P2_1$
Wavelength	0.9	0.9
Resolution	100-2.2	100-2.2
Cell dimensions		
a (Å)	86.9	86.9
b (Å)	277.8	278.1
c (Å)	92.9	92.9
α (°)	90.0	90.0
β (°)	117.6	117.6
γ (°)	90.0	90.0
Unique reflections	208106	210175
Completeness (%) (last shell)	99.0 (94.0)	92.9 (80.3)
R_{sym} (%) (last shell)[a]	7.0(2)	8.0 (55.0)
I/σ (last shell)	17.4 (2.2)	16.0 (2.0)
Multiplicity (last shell)	3.7 (3.0)	4.4 (2.5)
Refined model		
No. of residues	3720	3720
Water molecules	1217	1287
Resolution range (Å)	100–2.2	100–2.2
R_{fact} (%)	17.6	19.7
R_{free} (%)	22.2	22.9
Average *B*-factors (Å^2)		
Protein chains	AB 42.4, 43.2	AB 42.3, 42.5
	CD 42.6, 43.3	CD 42.2, 42.7
	EF 44.7, 44.0	EF 43.4, 43.2
	GH 47.1, 45.5	GH 42.2, 42.9
	IJ 47.7, 46.9	IJ 42.9, 42.4
	KL 48.4, 45.9	KL 42.9, 41.6
Waters	49.4	42.6
All atoms	30803	30992
Bond lengths (Å)	0.01	0.01
Bond angles (°)	1.33	0.91
Ramachandran plot (%)		
Preferred	89.3	89.3
Allowed	10.6	10.6
Outliers	0.1	0.1

[a] $R_{sym} = \Sigma_{hkl}\Sigma_{i=1}^{n}|I_{hkl,i} - \bar{I}_{hkl}|/\Sigma_{hkl}\Sigma_{i=1}^{n}I_{hkl,i}$.

Structural Analysis of the Influence of Residue 335 on Catalytic Properties toward Dibenzofuran—The average active site cavity volume of the $\alpha\beta$ dimers AB, CD, and EF of $BphAE_{RR41}$ was comparable with that of $BphAE_{p4}$ (17) (1073 Å^3 as calculated using CASTp program (37)). The corresponding atoms of the reactive ring of dibenzofuran and of biphenyl interact with the same residues of the α subunits of $BphAE_{RR41}$ and $BphAE_{LB400}$ (Gln^{226}, Phe^{227}, Asp^{230}, Met^{231}, Leu^{233}, Ala^{234}, His^{323}, and Leu^{333}), and they are located at approximately the same distances (not shown). Therefore, neither the overall size of the cavity nor the constraints on the reactive ring are affected by the mutations introduced in $BphAE_{RR41}$. The residues lining the distal portion of the $BphAE_{RR41}$ catalytic cavity are the same as those in $BphAE_{LB400}$ and $BphAE_{p4}$ (Phe^{384}, Phe^{378}, Val^{287}, Ser^{283}, Phe/Met^{336}, Leu^{333}, Gly^{321}, Tyr^{277}, His^{239}, Ala^{234}, and Met^{231}) (Fig. 5). However, the overall shape of the cavity of $BphAE_{RR41}$-dibenzofuran differs significantly from that of $BphAE_{LB400}$-biphenyl but is similar to that of $BphAE_{p4}$:2-chlorobiphenyl (Fig. 5). This is caused principally by the replacement of Phe^{336} by Met combined with the conformational freedom of Gly^{321}. The new catalytic properties of $BphAE_{p4}$ toward dibenzofuran (and in part those of $BphAE_{RR41}$) can thus be attributed to structural changes in the distal portion of the substrate-binding pocket. As noted for $BphAE_{p4}$, the T335A mutation relieves constraints on the Val^{320}:Gln^{322} segment, allowing

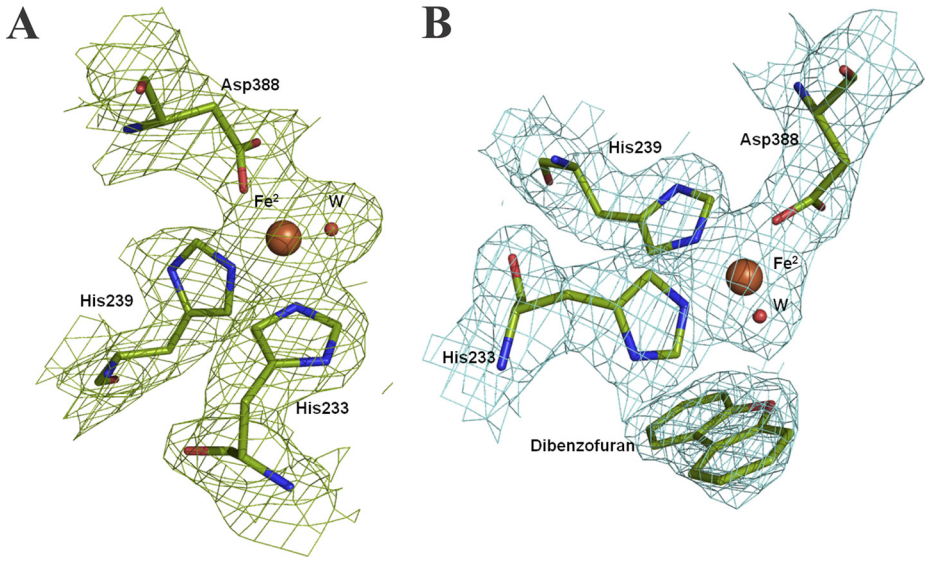

FIGURE 4. **The $2F_{obs} - F_{calc}$ electron density contoured at 1.0 σ level in the vicinity of the active site of chain AB from $BphAE_{RR41}$.** *A*, substrate-free. *B*, dibenzofuran-bound form.

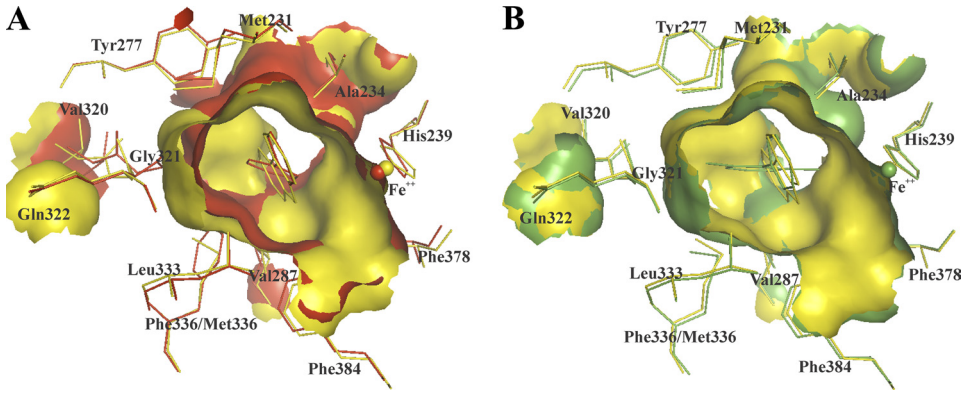

FIGURE 5. **Superposition of a portion of the catalytic cavity showing the residues lining the distal ring pocket.** Superposition of dimers AB of $BphAE_{RR41}$-dibenzofuran (*yellow*) and $BphAE_{LB400}$-biphenyl (*red*) (*A*) and $BphAE_{RR41}$-dibenzofuran (*yellow*) and $BphAE_{p4}$:2,6-dichlorobiphenyl (*green*) (*B*).

displacement of the Gly^{321} carbonyl such that it moves away from the substrate (17). In this case, the removal of Gly^{321} from dibenzofuran reduces the influence it exerts on the distal ring of the substrate. This is significant because dibenzofuran is obligatory co-planar: an altered placement of the distal ring would influence the orientation of the proximal ring inside the catalytic pocket.

Structural Analysis of the Influence of Residues 338 and 409 on Enzyme Stability—Based on the crystal structure of $BphAE_{RR41}$, as well as the structures of $BphAE_{LB400}$ and $BphAE_{p4}$ (17), Gln^{338} and Phe^{409} are too distant from each other to interact. To understand the effect of these two mutations,we need to examine closely the overall structure of the α and β subunits and the contacts at the $\alpha\alpha$, $\beta\beta$, and $\alpha\beta$ interfaces.

The overall crystal structure of the β subunit of $BphAE_{RR41}$ is very similar to that of other biphenyl dioxygenases (16, 17) and naphthalene dioxygenase (2). It includes a long twisted six-stranded β sheet, with three helices on the inward side of the sheet and a loop made of residues 9–20 (Fig. 6*A*) on its outward side. Many polar interactions are uniformly distributed between the β-sheet residues of vicinal β subunits and between two of the helices and β-sheet residues of the vicinal subunit. In addition, helix α3 and strand β2 are in contact with the α subunit. This suggests that the β subunit plays a key role in subunit assembly.

As reported for other dioxygenases (2, 16), the α subunit comprises two domains: the Rieske and catalytic domains. Unlike the β subunits, the crystal structures show unevenly distributed contacts between vicinal α subunits; these contacts occur principally at the junction between the Rieske domain of one α subunit and the catalytic domain of its vicinal subunit (Fig. 6*A*).

The Rieske domain is dominated by antiparallel β strands from which two hairpin structures protrude to form two fingers that hold the [2Fe—2S] center. The catalytic domain contains the catalytic Fe^{2+}, which lies against a eight-stranded antiparallel β sheet on one side and is surrounded on the other sides by helices and loops (Fig. 6*B*). Residues Arg^{101}, His^{102}, Arg^{103}, and Gly^{104} of the Rieske domain form the tip of hairpin 1. This short segment (in *blue* in Fig. 6, *B* and *C*) is embedded inside a matching trough of the vicinal α subunit; it faces helix α6 of the catalytic domain, comprised of residues Trp^{220} to Ser^{229}, and it also contacts a short segment (β21) comprised of residues Pro^{408}, Phe^{409}, and Asn^{410} and located at the edge of the catalytic domain. Agr^{103} forms a polar contact with Glu^{225} of helix α6. Arg^{101} forms polar contacts with Pro^{408} and Asn^{410}, and Arg^{104} forms a polar contact with Asn^{410} (Fig. 6*C*). Therefore, the crystal structures show that residue Phe^{409} is located within a stretch of amino acids that appears to play an important role in subunit assembly and/or in maintaining the stability of the oligomeric structure. In $BphAE_{RR41}$, Phe^{409} is ~4.6 Å from Phe^{222} of helix α6 (Fig. 6*C*). Alignment of dimers AB, CD, EF, GH, IJ, and KL of $BphAE_{RR41}$ and its dibenzofuran-bound form with dimers AB, CD, EF, GH, IJ, and KL of the substrate-free and bound forms of $BphAE_{LB400}$ or $BphAE_{p4}$ shows that Phe^{409} of $BphAE_{RR41}$ aligns very well with Leu^{409} of $BphAE_{LB400}$ or $BphAE_{p4}$ (not shown). In the latter enzymes, however, Leu^{409} is at an average distance of 5.4 Å from Phe^{222}. This could explain why replacing Leu^{409} of $BphAE_{p4}$ with a larger side chain in Phe^{409} suppresses the negative impact of the N338Q mutation on hexamer assembly. Through its interaction with Phe^{222}, Phe^{409} seems to help stabilize subunit assembly by reinforcing the role played by segment Pro^{408}–Asn^{410} in holding the subunits together.

Structural Analysis of the Influence of Residues 338 and 409 on Catalytic Properties—Prior studies identified mutations within a subsequence called region III that influenced the oxygenase's catalytic properties (12–14). This region includes a loop between strands β18 and β19 and a portion of strand β19. Residues 338 and 341 are both located on strand β19 (Fig. 6*C*). Superposition of the catalytic domains of $BphAE_{RR41}$ and $BphAE_{LB400}$ reveals minor variations in strand β19 that can be attributed to the longer side chain of Gln^{338} in $BphAE_{RR41}$ (not shown). Strand β19 faces helix α12, which interacts with the tip of hairpin-2 of the vicinal Rieske domain and includes iron ligand Asp^{388}. The tip of Rieske domain hairpin-2 includes Ser^{121}, Tyr^{122}, and His^{123}. These residues make polar contacts with Thr^{237} and Thr^{238} located at the junction between helices α7 and α8, on which are located iron ligands His^{233} and His^{239}. In addition, Ser^{121} and His^{123} make polar contacts with Gln^{226} and Asp^{230}, two residues believed to be involved in the reaction mechanism (36, 38) and found in the catalytic cavity at the level of the proximal ring of the substrate (17) (Fig. 6*B*). Furthermore, Tyr^{122} has a polar contact with Trp^{392} and Ser^{121} with Asn^{391} of helix α12. Gln^{338} forms two polar contacts with

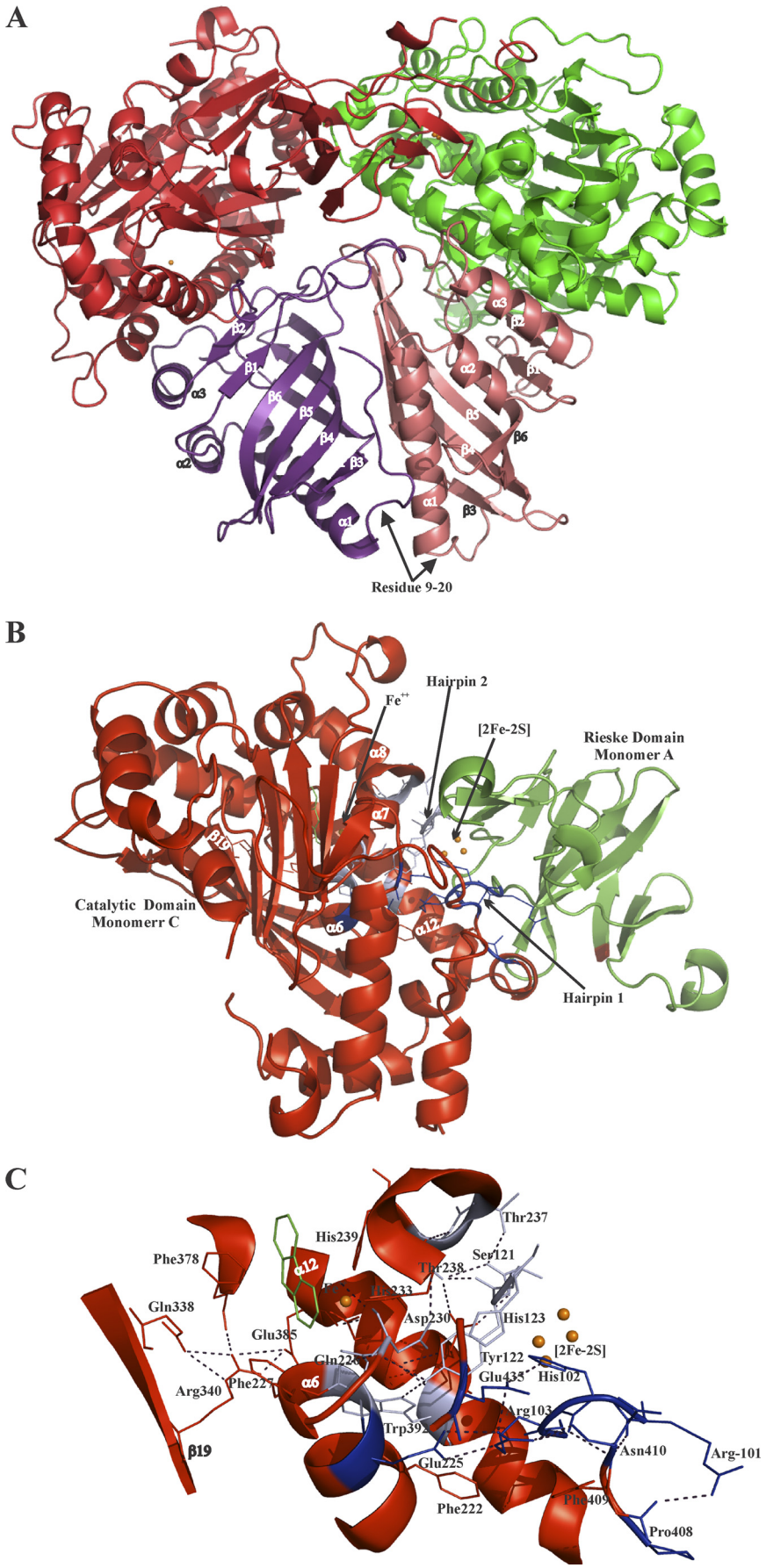
A
Residue 9-20
B
Hairpin 2
Fe++
[2Fe-2S]
Rieske Domain
Monomer A
Catalytic Domain
Monomerr C
Hairpin 1
C
Thr237
His239
Phe378
Ser121
Gln338
Asp230
His123
Glu385
[2Fe-2S]
Tyr122
Arg340
Phe227
Glu435
His102
Arg103
Asn410
Arg-101
Glu225
Phe222
Pro408

Arg^{340}, and the latter forms two polar contacts with Glu^{385} of helix α12. Arg^{340} is also close enough to Glu^{385} to form a salt bridge with this residue (Fig. 6*C*). Therefore, Arg^{340} and Gln^{338} are located such that their conformation can influence the distribution in the space of helices α12, α8, α7, and α6, which are critical for catalytic activity and subunit assembly.

Analysis of the crystal structure did not suggest a clear-cut mechanism by which Gln^{338} and Arg^{340} exert these effects. However, the longer length of the Gln^{338} side chain compared with Asn^{338} might disturb a key state not observed in the crystal or the internal dynamics of the protein. With respect to the latter possibility, it is clear from structural analysis that residues on helix α12 move considerably during substrate binding, showing that this protein segment is rather adaptable (Fig. 7). This movement is likely required to suitably align the reactive atoms for progression along the chemical reaction.

In ROs, the proximity between the Rieske cluster and the iron in the active site of the adjacent α subunit is consistent with a mechanism involving a transfer of electron across the interface between two subunits (2, 16, 17). This is corroborated by the fact that full activity requires that α and β subunits associate into a $\alpha_3\beta_3$ configuration (31). Such a mechanism must demand precise alignment of the amino acids involved in electron transfer between the Rieske cluster and the mononuclear iron of each adjacent α subunit, highlighting the importance of the protein atoms involved in the αα subunit interface.

Therefore, crystal structure analysis is consistent with an induced fit response required to reorganize the active site and facilitate the interplay between protein atoms critical for the reaction. The N338Q substitution might disturb the conformation of helices α12 and α6, resulting in subunit instability or misassembly. Conversely, the double Gln^{338} and Phe^{409} mutation may affect the conformational fluctuations of these helices in such a way that it enhances the roles of protein residues such as Asn^{388}, Gln^{226}, and Asp^{230} that are located on the helices and presumed to be involved in the chemical steps of the reaction (2, 38).

DISCUSSION

In this study, we examined the crystal structure of $BphAE_{RR41}$, an evolved RO that oxidizes dibenzofuran more efficiently than its $BphAE_{LB400}$ and $BphAE_{p4}$ parents. Despite the limitations of crystal structure analyses, the study revealed two pathways through which ROs evolve to expand their substrate range.

Traditionally, enzyme engineering to alter the substrate range involves mutations at residues lining the catalytic pocket. This approach has been applied successfully in many circumstances (39–45). Reducing the size of a side chain or altering charge distributions can generate enzyme with new catalytic properties.

However, other studies have shown that several residues not in direct contact with the substrate can significantly change the catalytic properties of biphenyl dioxygenase toward biphenyl analogs (21, 22, 44). In this work we confirm the importance of the T335A mutation. In altering the plasticity of the catalytic cavity, this mutation allows the carbonyl of residue Gly^{321} to move away from the substrate. In a previous work, we showed that this movement was required to increase the space available

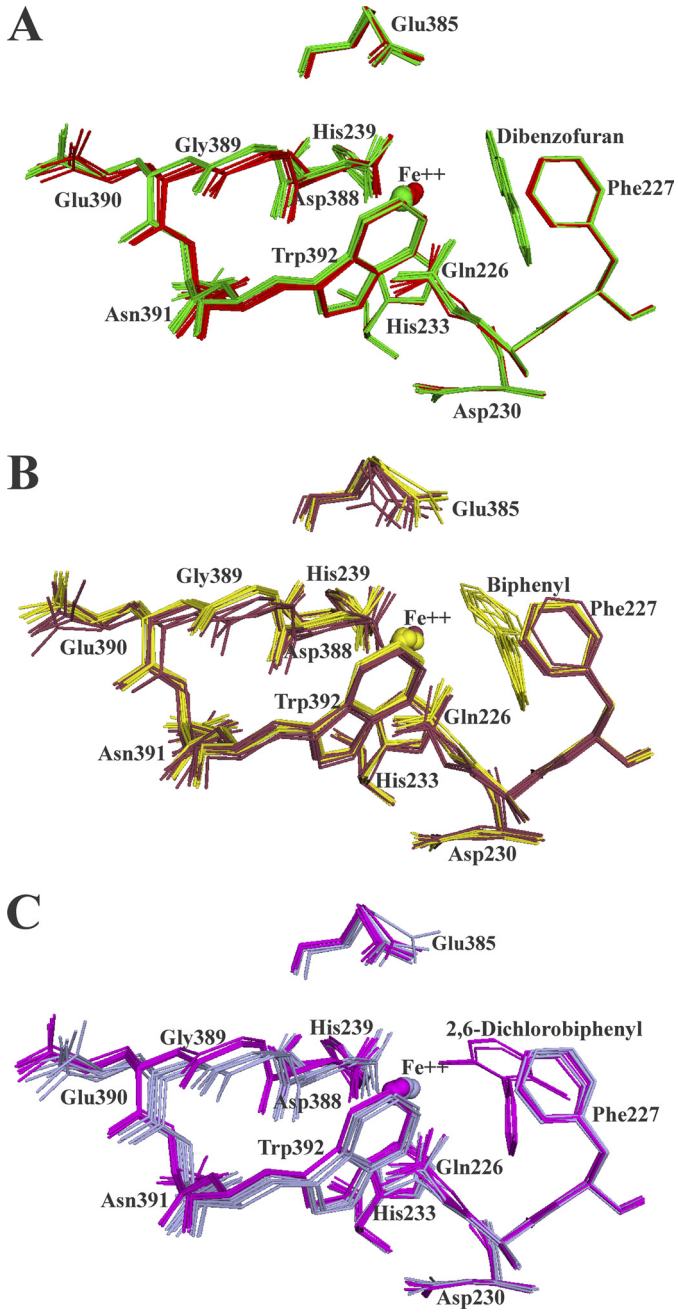

FIGURE 7. **Superposition of residues of the catalytic domain that move after substrate binding.** *A*, residues of $BphAE_{RR41}$ (*red*) and $BphAE_{RR41}$-dibenzofuran (*green*). *B*, residues of $BphAE_{LB400}$ (*brown*) and $BphAE_{LB400}$-biphenyl (*yellow*). *C*, residues of $BphAE_{p4}$ (*gray*) and $BphAE_{p4}$:2,6-dichlorobiphenyl (*purple*).

FIGURE 6. *A*, backbone ribbon drawing of the vicinal α/β dimers AB (*green* and *salmon*) and CD (*red* and *purple*) of $BphAE_{RR41}$-dibenzofuran highlighting the numerous contacts between two vicinal β subunits. *B*, ribbon drawing of the catalytic domain of monomer C (*red*) and of the Rieske domain of monomer A (*green*) of $BphAE_{RR41}$-dibenzofuran highlighting the interface between the two monomers. *C*, close-up view of the same interface shown in *B*. Hairpins 1 and 2 from the Rieske domains of monomer A (in *blue* and *gray*) protrude into a matching trough of the vicinal catalytic domain of monomer C. The residues from monomer C that contact the hairpins from the vicinal subunit are colored in *blue* or *gray* to match the residues they contact.

to bind the bulky 2,6-dichlorobiphenyl in a productive orientation (17). Because dibenzofuran is obligatory co-planar, any misplacement of the distal ring would influence the orientation of the proximal ring inside the catalytic pocket. Therefore, consistent with an induced fit mechanism, in $BphAE_{p4}$ and $BphAE_{RR41}$, the displacement of Gly^{321} appears to be required to reduce the influence it exerts through atomic interactions on the substrate's distal ring.

In this work, we highlighted a second and more subtle route to changes in substrate range, which implies that in ROs, either one or both of the induced fit or protein dynamic processes are involved to place the protein atoms involved in the reaction into proper relationships that facilitate catalysis. The reaction catalyzed by ROs is complex; it not only involves substrate binding and release of product, but also one dioxygen molecule is required in the reaction, and electrons must be transferred from the ferredoxin component to the Rieske cluster of one α subunit and then to the catalytic iron of the vicinal α subunit. Furthermore, a recent report showed residues at the interface between the Rieske domain and the catalytic domain move during formation of the complex between the oxygenase and ferredoxin components of carbazole 1,9a-dioxygenase (24). This implies that reaction-critical atoms from the Rieske domain must align properly with those of the vicinal catalytic domain, and the reaction-critical atoms of the catalytic domain must align properly to work together during the catalytic process. Structural analysis shows that residues located on secondary structures α6 and α12 are involved in subunit assembly, and biochemical data suggest that they are involved in the catalytic reaction (electron transfer and protonation) (2, 38). The fact that these residues move during substrate binding is consistent with a substrate-induced retuning process required to suitably align the protein atoms involved in the chemical steps of the reaction. In such a context, by altering the interactions occurring between secondary structure elements surrounding the catalytic center, the N338Q mutation generates a protein unable to stabilize the $\alpha_3\beta_3$ assembly previously shown to be required for activity (31). However, the double N338Q and L409F substitution generates an α subunit that supports a stable hexamer and where the retuning process is improved compared with its $BphAE_{LB400}$ and $BphAE_{p4}$ parents, resulting in a more efficient and faster catalytic reaction. ROs can thus be engineered to enhance their catalytic properties toward new substrates by altering the process involved in fine-tuning the interplay between the reaction-critical atoms.

Many questions remain unanswered; crystal structure analysis did not determine a clear-cut mechanism by which the double N338Q/L409F substitution affects the enzyme structure and catalytic properties, and our data do not determine which of the enzymatic steps are accelerated during the reaction. Although the data do not provide any direct demonstration that the N338Q and L409F substitutions either affect an induced fit or protein dynamic mechanism involved in the catalytic reaction, it is clear from crystal structure analysis that these residues occupy strategic positions whereby they can interact with reaction-critical protein atoms/groups and affect oligomeric assembly. Furthermore, residues of helix α12 and α6, and especially Asp^{388} and Gln^{226}, which are postulated to play a key role in the catalytic reaction (36), moved significantly during substrate binding in all variants ($BphAE_{LB400}$, $BphAE_{p4}$, and $BphAE_{RR41}$).

Altogether, our analysis shows that evolving ROs to change their substrate specificity is a rather complex enterprise that does not exclusively involve mutations at key residues in direct contact with the substrate. It appears that some mutations affect key residues associated with necessary conformational changes that are more difficult to identify by a rational approach but that are required to allow productive or improved interplay of reaction-critical atoms both inside and outside the substrate-binding pocket.

Acknowledgment—We appreciate the use of the SE Regional Collaborative Access Team 22-ID Beamline in the collection of x-ray diffraction data.

REFERENCES

1. Jakoncic, J., Jouanneau, Y., Meyer, C., and Stojanoff, V. (2007) *Biochem. Biophys. Res. Commun.* **352,** 861–866
2. Kauppi, B., Lee, K., Carredano, E., Parales, R. E., Gibson, D. T., Eklund, H., and Ramaswamy, S. (1998) *Structure* **6,** 571–586
3. Furukawa, K., Suenaga, H., and Goto, M. (2004) *J. Bacteriol.* **186,** 5189–5196
4. Haddock, J. D., Horton, J. R., and Gibson, D. T. (1995) *J. Bacteriol.* **177,** 20–26
5. Sylvestre, M. (2004) *Int. Biodeter. Biodegr.* **54,** 153–162
6. Chang, Y. S. (2008) *J. Mol. Microbiol. Biotechnol.* **15,** 152–171
7. Mohammadi, M., and Sylvestre, M. (2005) *Chem. Biol.* **12,** 835–846
8. Chun, H. K., Ohnishi, Y., Shindo, K., Misawa, N., Furukawa, K., and Horinouchi, S. (2003) *J. Mol. Catal. B Enzym.* **21,** 113–121
9. Seeger, M., González, M., Cámara, B., Muñoz, L., Ponce, E., Mejías, L., Mascayano, C., Vásquez, Y., and Sepúlveda-Boza, S. (2003) *Appl. Environ. Microbiol.* **69,** 5045–5050
10. Seo, J., Kang, S. I., Won, D., Kim, M., Ryu, J. Y., Kang, S. W., Um, B. H., Pan, C. H., Ahn, J. H., Chong, Y., Kanaly, R. A., Han, J., and Hur, H. G. (2011) *Appl. Microbiol. Biotechnol.* **89,** 1773–1782
11. Erickson, B. D., and Mondello, F. J. (1992) *J. Bacteriol.* **174,** 2903–2912
12. Mondello, F. J., Turcich, M. P., Lobos, J. H., and Erickson, B. D. (1997) *Appl. Environ. Microbiol.* **63,** 3096–3103
13. Barriault, D., Plante, M. M., and Sylvestre, M. (2002) *J. Bacteriol.* **184,** 3794–3800
14. Barriault, D., and Sylvestre, M. (2004) *J. Biol. Chem.* **279,** 47480–47488
15. Ferraro, D. J., Okerlund, A. L., Mowers, J. C., and Ramaswamy, S. (2006) *J. Bacteriol.* **188,** 6986–6994
16. Furusawa, Y., Nagarajan, V., Tanokura, M., Masai, E., Fukuda, M., and Senda, T. (2004) *J. Mol. Biol.* **342,** 1041–1052
17. Kumar, P., Mohammadi, M., Viger, J. F., Barriault, D., Gomez-Gil, L., Eltis, L. D., Bolin, J. T., and Sylvestre, M. (2011) *J. Mol. Biol.* **405,** 531–547
18. Suenaga, H., Goto, M., and Furukawa, K. (2001) *J. Biol. Chem.* **276,** 22500–22506
19. Suenaga, H., Mitsuoka, M., Ura, Y., Watanabe, T., and Furukawa, K. (2001) *J. Bacteriol.* **183,** 5441–5444
20. Suenaga, H., Nishi, A., Watanabe, T., Sakai, M., and Furukawa, K. (1999) *J. Biosci. Bioeng.* **87,** 430–435
21. Vézina, J., Barriault, D., and Sylvestre, M. (2007) *J. Bacteriol.* **189,** 779–788
22. Zielinski, M., Kahl, S., Hecht, H. J., and Hofer, B. (2003) *J. Bacteriol.* **185,** 6976–6980
23. Zielinski, M., Kahl, S., Standfuss-Gabisch, C., Cámara, B., Seeger, M., and Hofer, B. (2006) *Appl. Environ. Microbiol.* **72,** 2191–2199
24. Inoue, K., Ashikawa, Y., Umeda, T., Abo, M., Katsuki, J., Usami, Y., Noguchi, H., Fujimoto, Z., Terada, T., Yamane, H., and Nojiri, H. (2009) *J. Mol. Biol.* **392,** 436–451

25. L'Abbée, J. B., Barriault, D., and Sylvestre, M. (2005) *Appl. Microbiol. Biotechnol.* **67,** 506–514
26. Seeger, M., Cámara, B., and Hofer, B. (2001) *J. Bacteriol.* **183,** 3548–3555
27. Lin, J. J., Smith, M., Jessee, J., and Bloom, F. (1992) *BioTechniques* **12,** 718–721
28. Miroux, B., and Walker, J. E. (1996) *J. Mol. Biol.* **260,** 289–298
29. Sambrook, J., Fritsch, E. F., and Maniatis, T. (1989) *Molecular Cloning: A Laboratory Manual*, Cold Spring Harbor Laboratory Press, Cold Spring Harbor, NY
30. Laemmli, U. K. (1970) *Nature* **227,** 680–685
31. Hurtubise, Y., Barriault, D., and Sylvestre, M. (1996) *J. Biol. Chem.* **271,** 8152–8156
32. Haddock, J. D., and Gibson, D. T. (1995) *J. Bacteriol.* **177,** 5834–5839
33. Hurtubise, Y., Barriault, D., Powlowski, J., and Sylvestre, M. (1995) *J. Bacteriol.* **177,** 6610–6618
34. Imbeault, N. Y., Powlowski, J. B., Colbert, C. L., Bolin, J. T., and Eltis, L. D. (2000) *J. Biol. Chem.* **275,** 12430–12437
35. Kumar, P., Gómez-Gil, L., Mohammadi, M., Sylvestre, M., Eltis, L. D., and Bolin, J. T. (2011) *Acta Crystallogr. Sect. F Struct. Biol. Cryst. Commun.* **67,** 59–62
36. Karlsson, A., Parales, J. V., Parales, R. E., Gibson, D. T., Eklund, H., and Ramaswamy, S. (2003) *Science* **299,** 1039–1042
37. Dundas, J., Ouyang, Z., Tseng, J., Binkowski, A., Turpaz, Y., and Liang, J. (2006) *Nucleic Acids Res.* **34,** W116–W118
38. Parales, R. E., Parales, J. V., and Gibson, D. T. (1999) *J. Bacteriol.* **181,** 1831–1837
39. Bak-Jensen, K. S., André, G., Gottschalk, T. E., Paës, G., Tran, V., and Svensson, B. (2004) *J. Biol. Chem.* **279,** 10093–10102
40. Dietrich, M., Do, T. A., Schmid, R. D., Pleiss, J., and Urlacher, V. B. (2009) *J. Biotechnol.* **139,** 115–117
41. Huang, W. C., Westlake, A. C., Maréchal, J. D., Joyce, M. G., Moody, P. C., and Roberts, G. C. (2007) *J. Mol. Biol.* **373,** 633–651
42. Ostrander, E. L., Larson, J. D., Schuermann, J. P., and Tanner, J. J. (2009) *Biochemistry* **48,** 951–959
43. Parales, R. E., Lee, K., Resnick, S. M., Jiang, H., Lessner, D. J., and Gibson, D. T. (2000) *J. Bacteriol.* **182,** 1641–1649
44. Suenaga, H., Goto, M., and Furukawa, K. (2006) *Appl. Microbiol. Biotechnol.* **71,** 168–176
45. Xu, D., Enroth, C., Lindqvist, Y., Ballou, D. P., and Massey, V. (2002) *Biochemistry* **41,** 13627–13636